

SIMULATION OF AN INSTALLED PROPELLER BY MEANS OF STEADY AND UNSTEADY BODY-FORCE MODELING

Hugues Pantel¹, Fabrice Falissard¹ & Guillaume Dufour²

¹ONERA, Université Paris-Saclay, F-92190 Meudon, France ²ISAE-SUPAERO, Université de Toulouse, F-31055 Toulouse, France

Abstract

This work is dedicated to modeling a light propeller in isolated and installed configuration. The flow is modeled using three approaches, a blade-resolved Chimera method that is used as reference, and two types of body-force models based on the Blade Element Theory, one steady (RANS/BET) and one unsteady (actuator line).

Keywords: propeller, aerodynamics, body-force, actuator-line

1. Introduction

Reducing the fuel consumption of airliners is an increasingly important area of research, particularly to reduce greenhouse gas emissions. A way to do so is to improve propulsion system performance, in particular by increasing the engine by-pass ratio. Open rotors thus are good candidates to replace turbojets for mid-range airliners. Yet because of the absence of nacelle combined with the size of the engine, the aerodynamic interactions between the propulsive system and the airframe are significant. One of the challenges in developing this type of engine is to quantify the effects of propulsive integration on aircraft performance, i.e. to assess the impact of engine positioning on the flight envelope. It is therefore important to be able to account for the interaction between the engine and the airframe right from the design phase. To achieve this, numerical flow simulation methods are used, with more or less detailed modeling of the propulsion system depending on the purpose of the simulation (aircraft balance, aerodynamic forces computation, acoustic radiation). Today, two types of methods are favored for studying installation effects:

- Blade-resolved simulations, which model the flow around the rotating blades by solving the unsteady Navier-Stokes equations. This method provides an accurate description of the wake, but its computational cost can be prohibitive during the design phase.
- Simulations that do not solve the flow around the blades, but in which the rotor is modeled using source terms that are usually formulated as body-forces. This method significantly saves computation time compared to a full blade-resolved simulation since it avoids meshing the blades. However, this is gained at the cost of accuracy since the blade loads are computed using a model instead of using CFD.

Different methods exist to compute the body-forces. An option is to view the propeller as a whole and to compute the loads by considering the deviation and the losses in the flow through a blade row. Initially developed for turbomachinery [23], the model was recently adapted for propeller applications [9]. Another option to compute the body-forces is to express the loads of each isolated propeller blade using the Blade Element Theory (BET). The paper will focus in the following on methods based on the BET.

Steady body-force models, which average the rotor effects over a revolution in an actuator-disk-like computation, are already widely used in the aircraft industry today [15, 18]. However these models

do not capture the unsteady aspects of the flow, such as the blade tip vortices. An unsteady body-force model, the actuator line model, in which the source terms are placed in proximity of each blade, was developed to model the tip vortices [22]. First developed in the wind turbine field, the model is now being adapted to aeronautical needs, especially for helicopter applications [14]. Few propeller applications exist, and most are either used with a prescribed loading [21] or with loads interpolated from 3D blade-resolved computations [24], and not fully coupled with interpolations in a 2D airfoil polar database as in the original actuator line model.

This paper aims to present a steady and an unsteady fully coupled body-force method for propeller and open rotor modeling, based on the BET. The models are evaluated on a three-bladed propeller in isolated and installed configuration. The results are compared to reference blade-resolved computations.

2. Configurations and Operating Point

2.1 Isolated Propeller

The propeller geometry studied in this paper is the ONERA HAD-1 Propeller [15] pictured in Figure 1. It is a three-bladed light propeller with a radius R of 0.8m, a max chord length c_{max} of 0.124m, and a hub-to-tip ratio of 0.15. Unless specified otherwise, a 45° blade pitch angle is chosen at 75% of the propeller's radius. The cruise operating point is detailed in Table 1.



Figure 1 – HAD-1 propeller.

Table 1 – HAD-1 cruise operating point

| Parameter | Value |
|---------------------------------|--------|
| Free flow Mach number | 0.3 |
| Angle of incidence, ° | 0 |
| Air temperature, K | 288.15 |
| Air density, kg.m ⁻³ | 1.225 |
| Rotation speed, rpm | 2031 |

2.2 Installed Configuration

The installed configuration geometry is made up of the HAD-1 propeller with a straight wing behind it, as shown in Figures 2 and 3. The wing geometry parameters are detailed in Table 2. The leading edge is located 0.75R behind the rotation center in the X direction and 0.6R above the rotation center in the Z direction. The wing is thus sufficiently long to limit the effect of the wing tip vortices in the propeller wake, and close enough to the propeller so it interacts significantly with the propeller slipstream. The operating point is the same as for the isolated configuration.



Figure 2 – Installed configuration.

3. Computational Methodologies

3.1 Blade-Resolved Approach

The blade-resolved computations are performed using the finite-volume solver elsA [1], considering the unsteady Reynolds-Averaged Navier-Stokes (RANS) equations in compressible regime. The computations rely on a Chimera approach [17] in which structured body-fitted meshes are immersed in a background Cartesian grid (Figure 4). The hub mesh and the three blade meshes rotate at each time

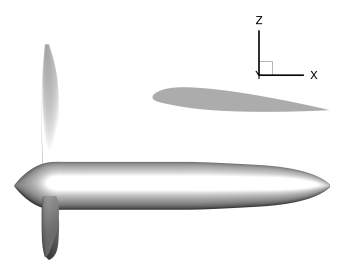


Figure 3 – Installed configuration – side view.

Table 2 - Wing geometry

| Parameter | Value |
|----------------|-----------|
| Airfoil | NACA23012 |
| Span, m | 10.0 |
| Chord, m | 1.0 |
| Pitch angle, ° | 4.0 |

step. Conservative variables are passed from one mesh to the other by interpolation. The main computational cost of this method comes from the interpolation coefficients that need to be recomputed at each time step.

The blade meshes have 4 million cells each and the hub mesh 5 million cells. An 8 million-cell body fitted wing mesh is added for the installed configurations. In both cases, the same background grid is used. It contains 80 million cells to preserve the blade tip vortices accurately for at least 2.5 propeller radii, where the cell dimension is equal to $c_{max}/15$.

For the CFD computations, the convective fluxes are discretized using a second-order centered scheme with scalar artificial viscosity [6] and Martinelli's correction [11]. The time discretization relies on a second-order three-time-level implicit backward-difference scheme. The time-step was chosen so the propeller rotates half a degree at each iteration. The turbulence modeling relies on a $k-\omega$ Kok turbulence model [10] with shear-stress transport (SST) correction [13].

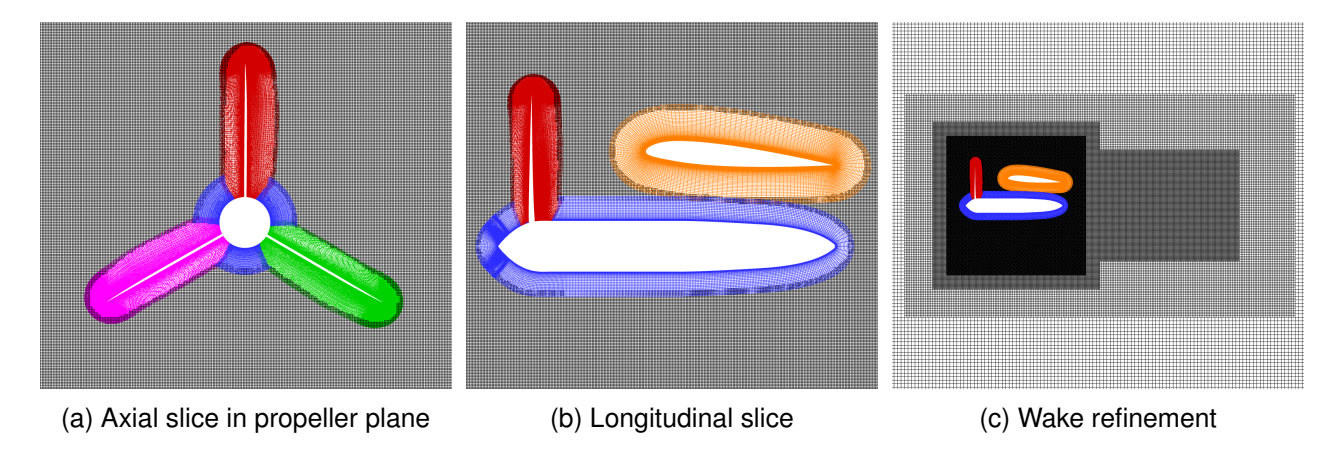
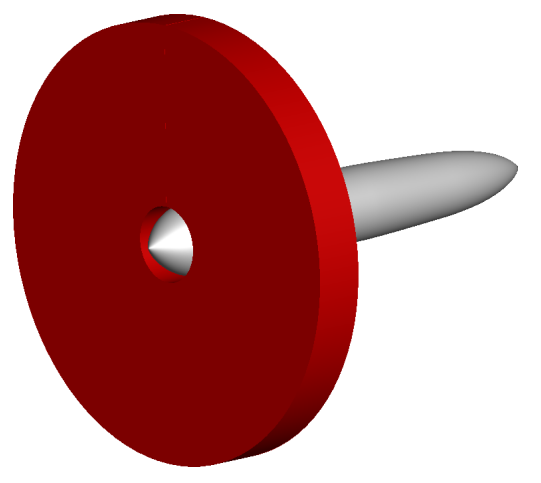


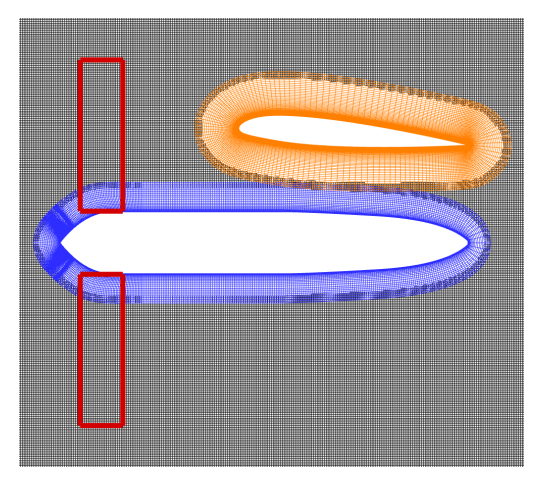
Figure 4 – Blade-resolved Chimera mesh.

3.2 Steady Body-Force Approach – RANS/BET Model

The steady body-force computations are conducted using the RANS/BET model as described by Pantel et al. [16]. This method is based on a full coupling between CFD and the Blade Element Theory (BET). The approach models the effect of the propeller by calculating body-forces using the local flow from CFD and the BET approach. The body-forces are accounted for in the computation as source terms distributed in a cylindrical volume centered around the rotation plane. The model thus only computes the time-averaged component of the flow and requires a tip-loss correction. The correction used in this paper includes an induced-velocities correction from Glauert [4] implemented using an iterative procedure described by Shen et al. [19]. An additional calibrated correction directly applied on the BET loads is also used, as described by Pantel et al. [16].

The computational mesh used for this approach is the same one as for the blade-resolved computation but without the body-fitted blades. Figure 5 shows the volume in which the source terms are distributed and a slice of the computational grid of the installed configuration.





- (a) Volume in which source terms are injected
- (b) Slice of the RANS/BET Chimera mesh.

Figure 5 – RANS/BET body-force model setup.

3.3 Unsteady Body-Force Approach – Actuator Line Model

The RANS/BET method presented previously only computes the time-averaged flow field, meaning that the resulting flow is smeared across the propeller disk. There are no blade-to-blade variations such as individual blade wakes or tip vortices. As a consequence, the method cannot represent the helical structure of the real wake. To overcome this limitation, an extended three-dimensional actuator disc model was developed by Sørensen and Shen [22], called the actuator line. In this model, the source terms are distributed along the blade positions and they rotate in the background mesh. This enables the study of the dynamic wake and of the tip vortices. The model was initially developed for wind turbine applications, where having an accurate representation of the turbine wakes improves the accuracy for wind farm analysis.

In the original model, velocities are sampled in the flow field computed by CFD on lines, called actuator lines, located at the blade positions (Figure 6a). Blade loads are then computed on these lines using BET, in the same manner as for the RANS/BET model. The main difference with the steady model comes from the fact that the source terms are then distributed very locally in the close proximity of each actuator line (Figure 6b). This is done using a 3D Gaussian projection kernel *g*:

$$g_{3D}(x,y,z) = \frac{1}{\varepsilon^3 \pi^{3/2}} \exp\left(-\frac{(x-x_0)^2 + (y-y_0)^2 + (z-z_0)^2}{\varepsilon^2}\right)$$
(1)

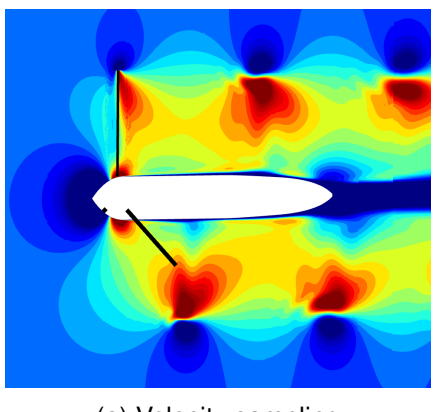
where (x_0, y_0, z_0) are the actuator line point coordinates, (x, y, z) are the CFD mesh coordinates, and ε is the Gaussian smearing width parameter.

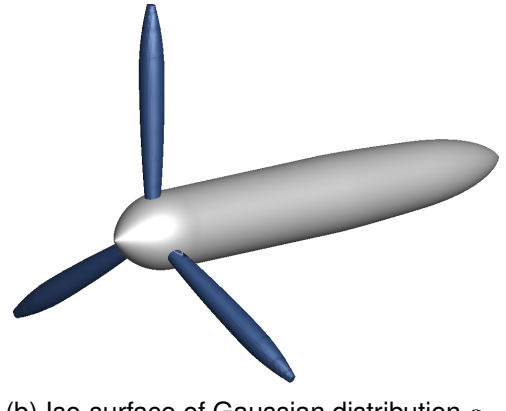
This model was reported in literature to consistently overestimate the loads at the tip of the blade, because the 3D Gaussian spreads source terms beyond the rotor radius [8]. Indeed, this smears the tip vortex over a larger volume and decreases the induced velocities at its center, leading to larger angles of attack and higher BET loads at the tip. The model is also very sensitive to the choice of ε , which is critical to the stability of the computation and to the correct prediction of blade loads [20].

To curb the limitations described above, the present model proposes to distribute the source terms using a 2D Gaussian at a constant radius to avoid smearing the loads over the propeller radius and thus limit the over-prediction of loads at the tip. The velocities used for the BET computations are also locally averaged using the same 2D Gaussian to avoid instabilities [3]. In these simulations the Gaussian parameter ε is linked to the chord of the blade c, as suggested by Shives and Crawford [20].

$$g_{2D}(r,\theta,x) = \frac{1}{\varepsilon^2 \pi dr} \exp\left(-\frac{(x-x_0)^2 + (r\theta - r\theta_0)^2}{\varepsilon^2}\right)$$
 (2)

where
$$\varepsilon/c = 0.3$$
 (3)





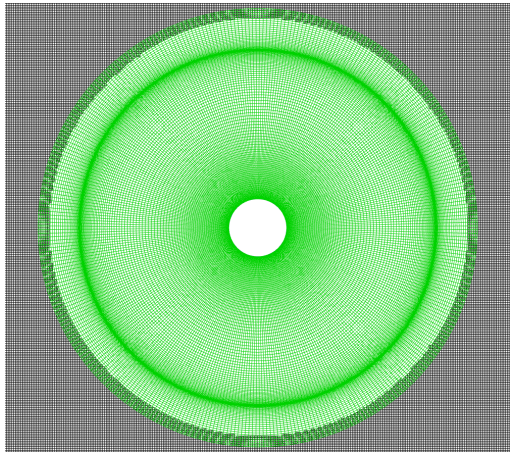
(a) Velocity sampling

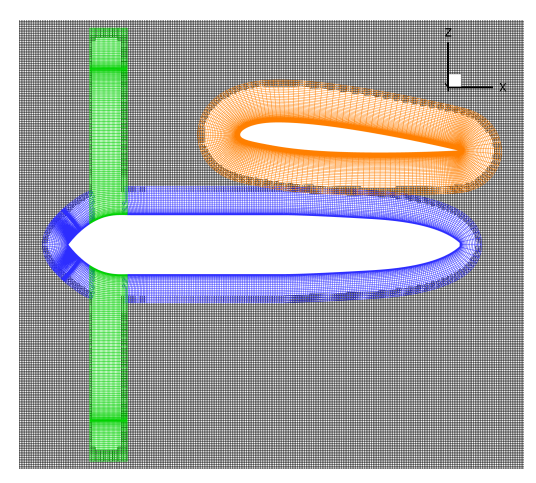
(b) Iso-surface of Gaussian distribution g_{2D}

Figure 6 – Actuator Line method.

The computations are conducted on the same background mesh as for the blade-resolved and steady body-force computations. This choice ensures that the differences observed in the wake velocity fields are only due to the method used to impose the circulation in the fluid and not related to differences in the computational grid.

The source terms are injected in an additional Chimera cylindrical grid, as shown in Figure 7. This grid has no movement, it is the source terms that rotate within the grid, so the actuator line computation can be conducted without having to recompute the interpolation coefficients at each iteration, and thus offers a significant cut in computation time compared to the blade-resolved computations. The cylindrical grid has 360 cells in the azimuthal direction and the computational timestep is of one degree so the actuator line points are always located on the grid cell centers. This cylindrical grid is the direct support of the actuator lines, meaning that each cell with an actuator line going through its center is an actuator line computation point. A non-uniform refinement is applied in the radial direction to better capture the strong load variation near the tip of the blade, as well as the tip vortices. This mesh goes down to the hub surface so source terms are injected down to the hub boundary layer. This prevents vortices from developing between the hub and the root of the actuator lines which do not exist in the blade-resolved computations.





(a) Axial slice in the actuator line plane

(b) Longitudinal slice

Figure 7 – Actuator line mesh.

4. Results for the Isolated Configuration

This section is dedicated to the modeling of the isolated propeller configuration presented in section 2.1. Detailed results are first given for a 45° blade pitch angle, and propeller characteristics are then presented for each modeling method.

4.1 Design Point

The results presented in this section were obtained with the isolated propeller configuration at the operating point from Table 1. The integrated loads, obtained for each propeller modeling method, are shown in Table 3. The RANS/BET model predicts the thrust and power quite accurately thanks to the calibrated tip-loss correction. The actuator line model overestimates these quantities by around five percent. The error is however consistent for thrust and power so the efficiency prediction is accurate.

| Modeling method | Thrust [N] | Power [kW] | Efficiency |
|-----------------|--------------|---------------|-----------------|
| Blade-Resolved | 1406 | 166.8 | 0.860 |
| RANS/BET | 1437 (+2.2%) | 167.3 (+0.3%) | 0.877 (+1.7pts) |
| Actuator line | 1480 (+5.2%) | 175.1 (+5.0%) | 0.863 (+0.3pts) |

Table 3 – Integrated loads for each approach

Figure 8 shows the spanwise distribution of axial and tangential loads along the blade for each method. For the thrust, both body-force methods give a good prediction on the inner part of the blade and overshoot the loads near the tip. For the RANS/BET model, this shows that the calibrated tip-loss correction could be further refined, but it still yields good results for the tangential loads. For the actuator line model, the over-prediction at the tip is a common phenomenon [5, 12]. Its origin is most likely linked to the Gaussian smearing of the source terms, as explained in section 3.3. The results presented here indicate that the use of a 2D Gaussian is not enough to completely avoid the overshoot. Literature shows that using a smaller Gaussian parameter can reduce the tip loads [7], but it requires a finer mesh capable of correctly discretizing the smearing function [2]. Such meshes were not investigated in this work as the extra cost due to the larger mesh would compensate the cost saved by the body-force method.

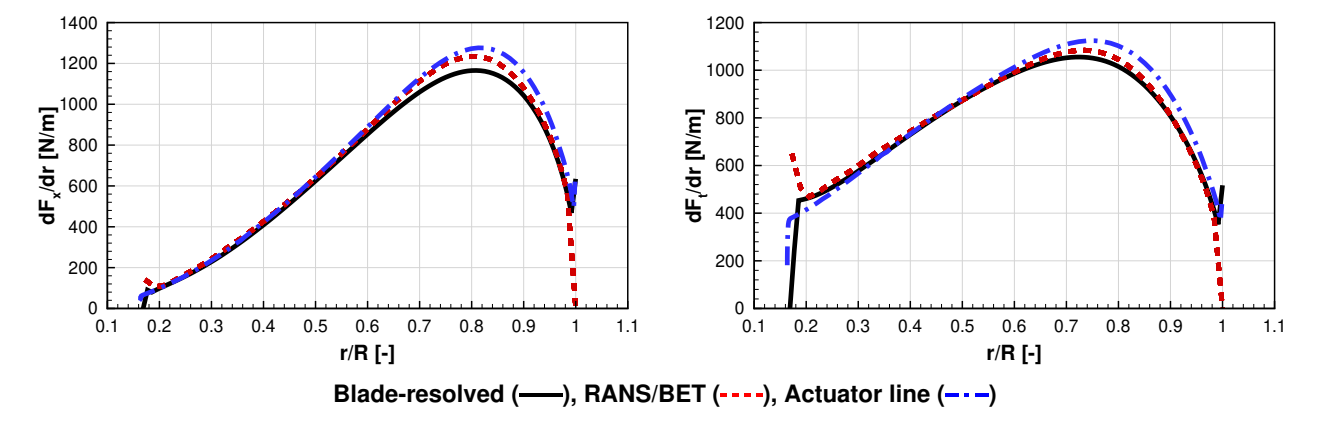


Figure 8 – Axial and tangential spanwise blade loads computed by the three methods.

4.2 Propeller Pitch Variation

The actuator line model was used to evaluate propeller performance at different blade pitch angles, using the setup described in section 3.3. The results are compared to the propeller characteristics computed by Pantel et al. [16] using a blade-resolved and RANS/BET approach. The setups used differ slightly from the ones from sections 3.1 and 3.2 (no Chimera mesh and different hub shapes), but the operating point and the RANS/BET model are identical.

The propeller thrust, power and efficiency as a function of blade pitch angle and thrust are plotted in Figure 9. The thrust and power curves show that the 5% overestimation seen at a 45° pitch angle is about the same for all pitch angles, leading to a very good prediction of propeller efficiency for all pitch angles as well. This is important because the aim of the actuator line method developed here is to study installation effects, in which the input is often the thrust rather than the blade pitch angle. As a result if the propeller is trimmed for thrust, the propeller power will also be correct, and so will the tangential loads that put the fluid in rotation. This would not be the case as much for the RANS/BET

model, which predicts the thrust and power more accurately than the actuator line model for a given pitch angle, but is off on the efficiency characteristic by about one point.

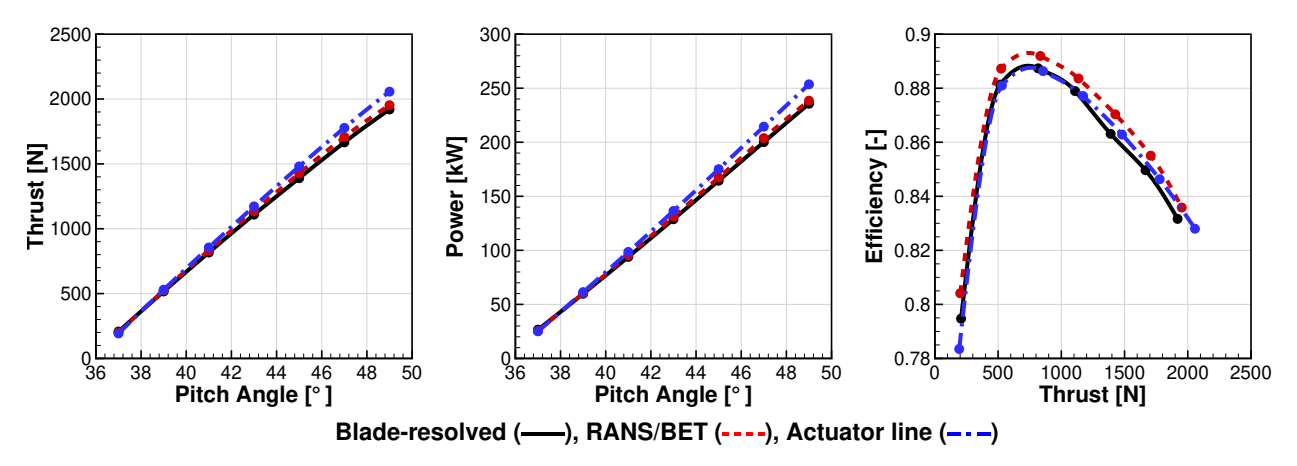


Figure 9 – Propeller characteristics.

5. Results for the Installed Configuration

This section presents the conclusions of the computations run on the installed configuration presented in section 2.2. The wing induces an up-wash in the propeller plane, leading to an unsteady blade load over a revolution. Likewise, the tip vortices shed by the propeller periodically hit the wing, inducing unsteady wing loads as well. The first subsection presents results that are time-averaged and that allow a three-way comparison between the blade-resolved, RANS/BET, and actuator line computations. The second subsection focuses on the unsteady flow and thus only compares blade-resolved and actuator line results.

5.1 Mean Flow

The time-averaged propeller and wing loads are presented in Table 4. For the actuator line model, the thrust and power overestimations are consistent with the results from the previous section. However the RANS/BET method is not as precise as for the isolated configuration, indicating the model may not account for the impact of the wing up-wash well. The variation of the blade load over a rotation also leads to the appearance of an in-plane (1P) force that is displayed in Table 4 as a modulus and a phase angle (angle between the 1P vector and the Z axis). The in-plane force is very well predicted by the actuator line model. The RANS/BET largely overestimates the modulus despite being accurate on the phase angle. The average wing lift and drag coefficients are all very close because the perturbation created by the propeller tip vortices only affects a relatively small portion of the wing.

| Quantity | Prop off | Blade-resolved | RANS/BET | Actuator line |
|--------------|----------|----------------|-------------------|-----------------|
| Thrust [N] | - | 1492 | 1561 (+4.6%) | 1562 (+4.7%) |
| Power [kW] | = | 173.5 | 176.3 (+1.6%) | 181.3 (+4.5%) |
| Efficiency | = | 0.878 | 0.904 (+2.6pts) | 0.880 (+0.2pts) |
| 1P Loads [N] | - | 54 | 74 (+37.8%) | 56 (4.8%) |
| 1P Phase [°] | - | 14.4 | 13.2 (-1.2°) | 13.4 (-1°) |
| Wing CI | 0,45838 | 0,45828 | 0,458856 (+0.13%) | 0,45822(-0.01%) |
| Wing Cd | 0,01621 | 0,01686 | 0,016818 (-0.27%) | 0,01685(-0.07%) |

Table 4 – Propeller and wing performance averaged over a full rotation

Figure 10 shows the azimuthal variation of blade thrust and power over a revolution for the three methods. Both body-force methods reproduce the general blade-resolved trends accurately, including the azimuths at which the maximum and minimum thrust and power are reached. The actuator line thrust and power curves are offset compared to the blade-resolved results by around +5%. The

RANS/BET model is less consistent, by overshooting and undershooting the loads depending on the azimuth.

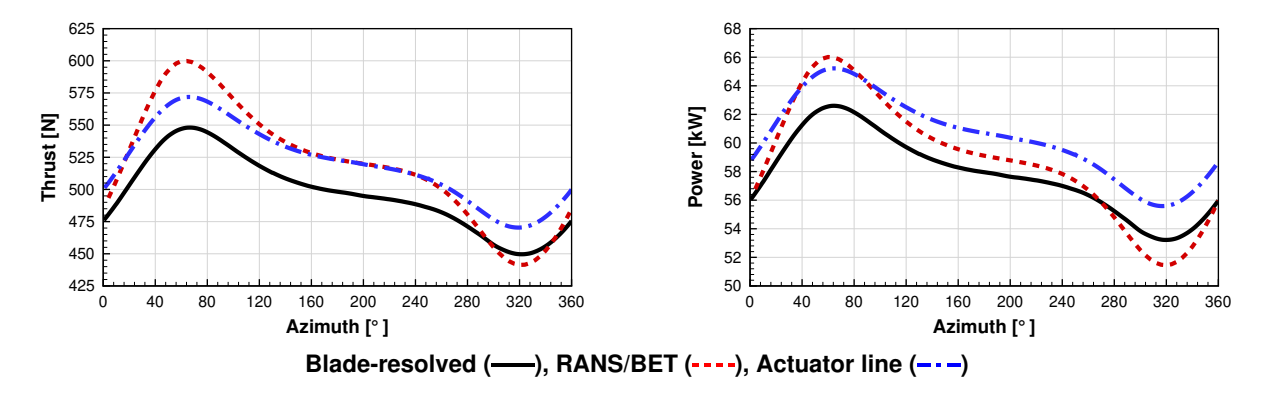


Figure 10 – Blade axial and tangential loads over a revolution.

Details into the spanwise loads are given in Figures 11 and 12, which show the axial and tangential loading disks over a revolution. Just like for the isolated propeller case, both body-force methods give a nearly perfect prediction on the inner part of the blade, at all azimuths. On the rest of the blade, the actuator line model consistently overestimates the max tip load by around 5%. The RANS/BET model is more accurate on the lightly loaded azimuths and less accurate when the blade is more loaded.

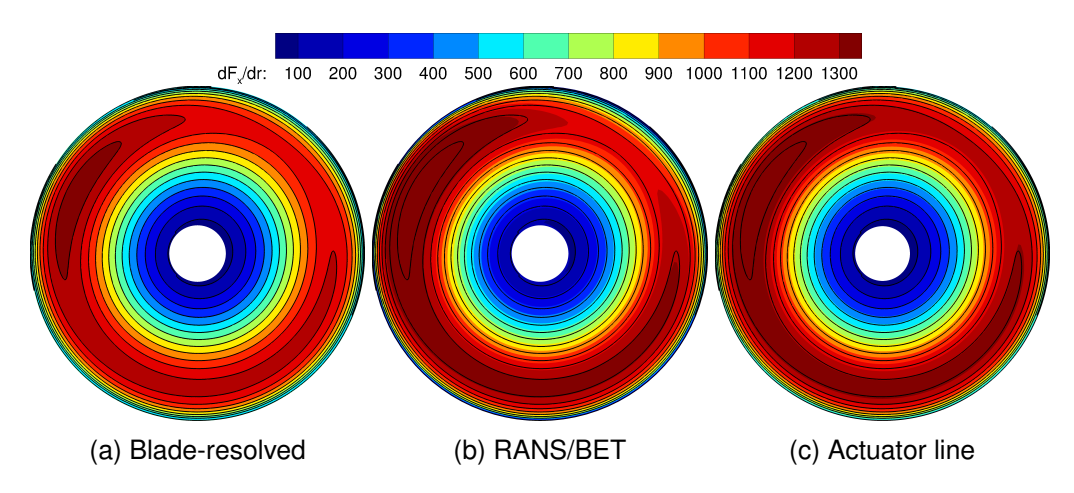


Figure 11 – Distribution of blade axial loads over a revolution, in N/m.

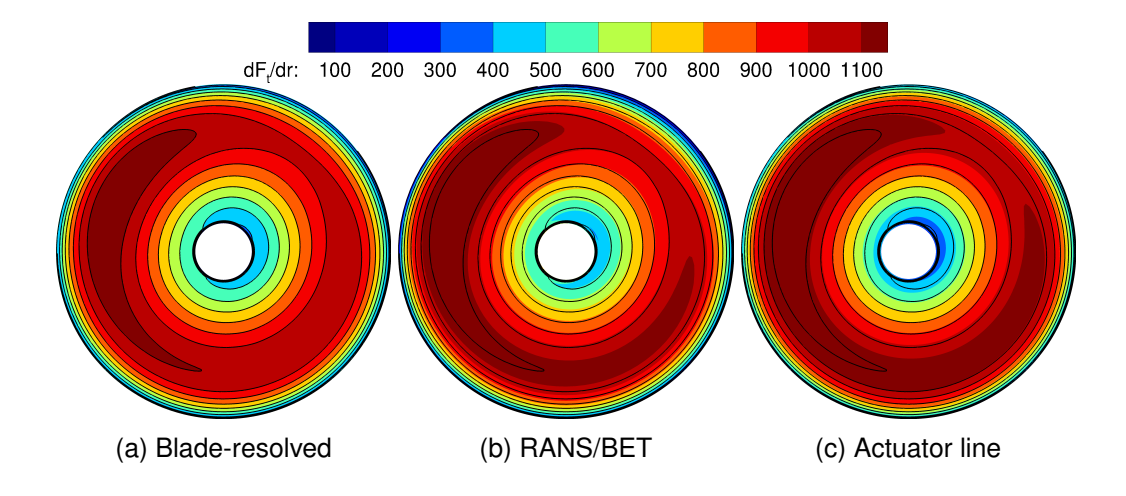


Figure 12 – Distribution of blade tangential loads over a revolution, in N/m.

The results show that the actuator line method accurately follows all the blade-resolved spanwise and azimuthal trends, indicating that the presence of the wing is correctly accounted for in the computation. However the model consistently overestimates the blade tip maximum load by around 5%, leading to an overestimation of blade thrust and power by also 5% for all azimuths. The explanation for this is probably the same as for the isolated propeller case, ie. the smearing of the loads by the Gaussian kernel which creates less induction at the blade tip.

The RANS/BET model, which was effective in the isolated configuration, does not predict the azimuthal load variation so accurately. This is most likely due to the tip-loss correction used. The induced-velocities correction used here [19] was designed for axisymmetric flow, where the velocity induced by the propeller can be obtained by subtracting the axial freeflow component from the field solved by CFD. This correction can be easily adapted for propellers under incidence for which the field to subtract to obtain the propeller induced velocity field is still well defined. This adaptation to flows under incidence was already successfully made for the RANS/BET model [16]. However for installed configurations, the flow used to compute the tip-loss correction does not only include the velocity induced by the propeller, but also the velocity induced by the wing, thus distorting the correction and the loads at the tip of the blade. Since the velocity induced by the wing is not the same in the blade frame at all blade azimuths, this explains why the load prediction accuracy is highly dependent on the blade position. A RANS/BET tip-loss correction adapted to installed case will be investigated in future work.

Despite the limitations described above, both body-force approaches give a very accurate prediction of the average spanwise lift and drag of the wing, displayed in Figure 13. The first thing to note is that the RANS/BET model does give a wing loading that is similar to the time-averaged loadings of the actuator line and blade-resolved approaches. Because of its direction of rotation, the propeller wake creates an up-wash on the left side of the wing and a down-wash on its right side, thus explaining the general shape of the spanwise lift curves. The slight amplitude overshoots by the actuator line model are caused by the propeller tip vortices which are stronger because of the overestimated blade loads.

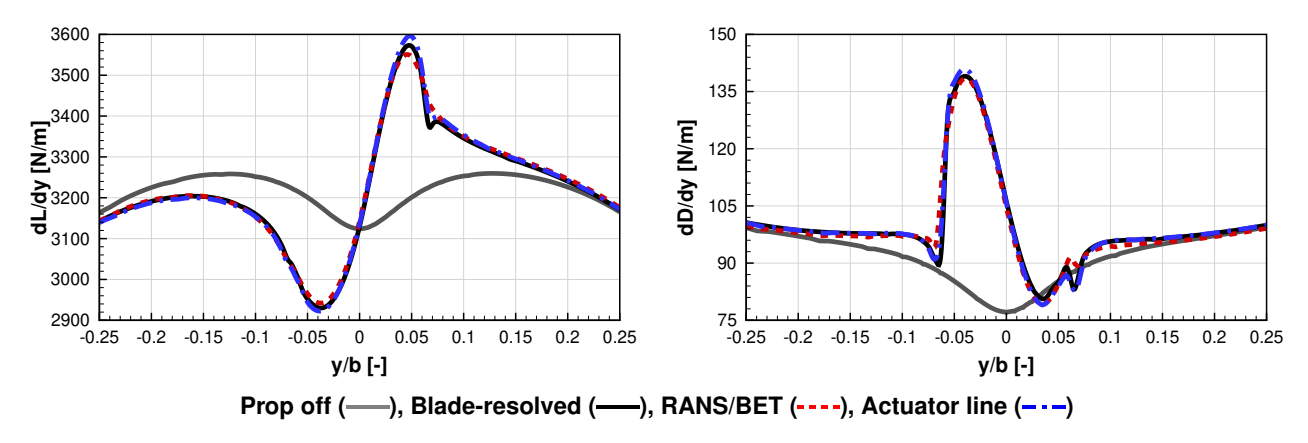


Figure 13 – Wing spanwise lift and drag averaged over a revolution.

5.2 Unsteady Flow

This section focuses on the unsteady aspects of the blade-resolved and actuator line computations. Figure 14 shows Q-criterion iso-surfaces for a time step where a blade tip vortex hits the blade, for the blade-resolved and actuator line computations. The vortex-systems seem very similar.

Figure 15 shows the total wing lift and drag as a function of a reference blade position, 0° corresponding to a blade aligned with the Z axis (defined in Figure 2). The loads are 120°-periodic so the study only focus on a third of a revolution. The curves for the two modeling methods are in phase, but the actuator line amplitude is slightly higher due to the overestimated blade loads.

Figures 16 and 17 show spanwise wing loads, focusing on the area most affected by the propeller wake. Figure 16 shows the wing lift at timesteps for which the lift is the highest and the lowest. Figure 17 shows the wing drag at timesteps for which the drag is the highest and the lowest. For all cases, the actuator line model is able to capture the correct trends with a great precision, even

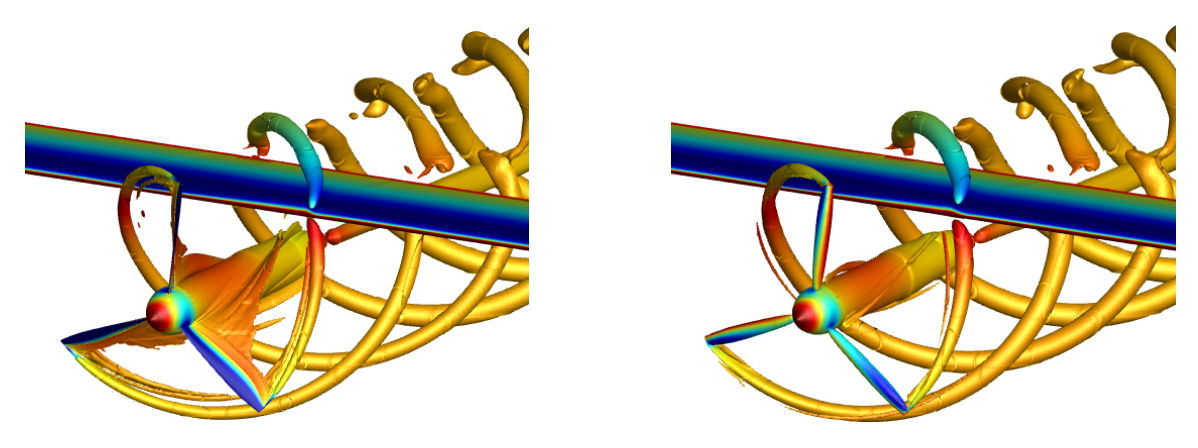


Figure 14 – Iso-Q-citerion for the blade-resolved (left) and actuator line (right) computations, colored by pressure.

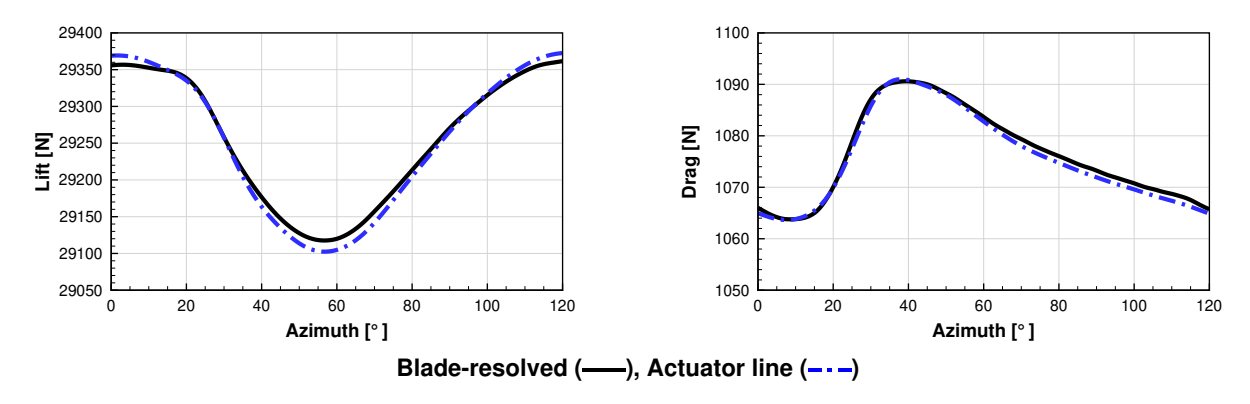


Figure 15 – Wing lift and drag as a function of blade azimuth.

though the loading profiles can vary significantly in time (especially for the drag). A reason the body-force model seems to work so well also comes from the blade-resolved solution: the viscous wakes shed by the blades cannot be fully conserved until they reach the wing, this would require an unreasonably large mesh. As a result, even in the blade-resolved simulation, mostly the potential effects are captured. The actuator line model is incapable of modeling the viscous wake because no boundary layer is formed without the blade surfaces, so only the potential effects are modeled with this approach as well. This can be seen on Figure 14 where the blades' viscous wakes can only be seen in the blade-resolved simulation, and are mostly dissipated before they can reach the wing.

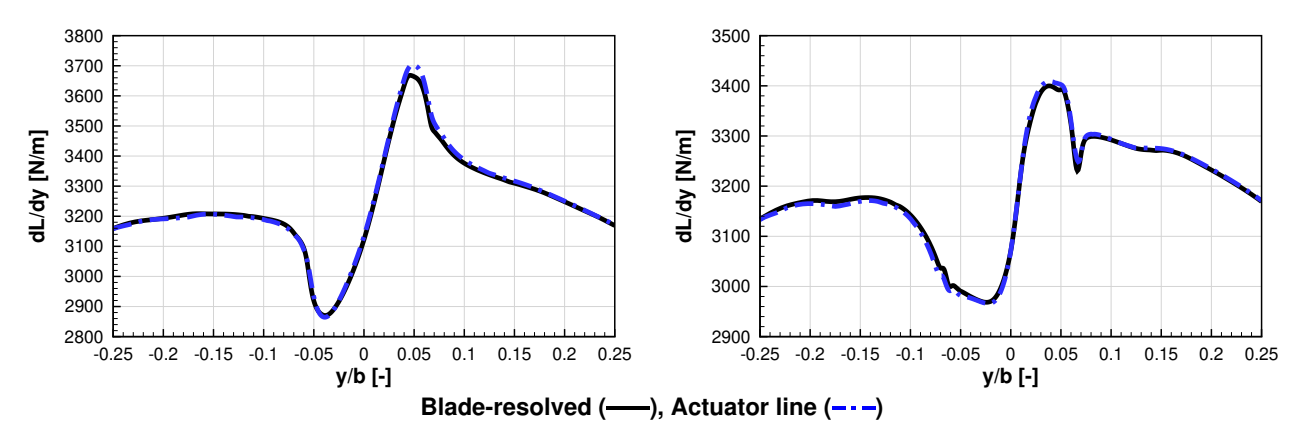


Figure 16 – Wing spanwise lift distribution for azimuths where integrated lift is maximum (left) and minimum (right).

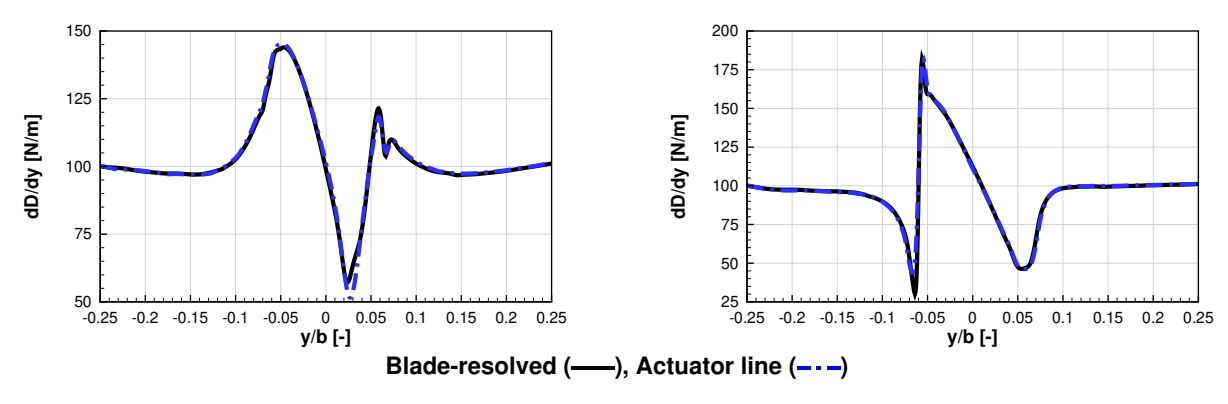


Figure 17 – Wing spanwise drag distribution for azimuths where integrated drag is maximum (left) and minimum (right).

6. Conclusions

This work is dedicated to modeling a light propeller in isolated and installed configuration. The flow is modeled using three approaches, a blade-resolved Chimera method that is used as reference, and two types of body-force models that rely on a coupling between the Blade Element Theory and CFD. The body-force approaches include a steady model, called RANS/BET, that averages the propeller effect on a whole revolution, and an unsteady actuator line model that distributes the source terms in proximity of each blade position.

In the isolated configuration, the RANS/BET model predicts propeller thrust by around 2% and power by less than 1%. The actuator line model overestimates both by 5% because of an overloaded blade tip. These differences stay constant with blade pitch angle variation. In the installed configuration, the accuracy of the RANS/BET prediction of the blade loads varies with the azimuth, whereas the actuator line model consistently overestimates blade loads by 5%, regardless of the azimuth. However, both body-force models are able to evaluate the wing load very precisely, whether it is the average loads for the RANS/BET model and the actuator line model, or the unsteady loads for the actuator line model.

Future work will include a more in-depth investigation into the RANS/BET model tip-loss correction for installed configurations, to better predict the azimuthal variation of the blade loads. An actuator line computation in which the propeller is trimmed for thrust will also be studied, to see if this can remove the slight differences in unsteady wing loads that remain.

Acknowledgments

This project has received funding from the Clean Sky 2 Joint Undertaking (JU) under grant agreement No 945583. The JU receives support from the European Union's Horizon 2020 research and innovation programme and the Clean Sky 2 JU members other than the Union. The results, opinions, conclusions, etc. presented in this work are those of the author(s) only and do not necessarily represent the position of the JU; the JU is not responsible for any use made of the information contained herein. This research has also received funding from the research program CLEOAPTRA, partly supported by the French civil aviation directorate through the France 2030 plan.

Contact Author Email Address

Corresponding author: Fabrice Falissard, fabrice.falissard@onera.fr

Copyright Statement

The authors confirm that they, and/or their company or organization, hold copyright on all of the original material included in this paper. The authors also confirm that they have obtained permission, from the copyright holder of any third party material included in this paper, to publish it as part of their paper. The authors confirm that they give permission, or have obtained permission from the copyright holder of this paper, for the publication and distribution of this paper as part of the ICAS proceedings or as individual off-prints from the proceedings.

References

- [1] L. Cambier, S. Heib, and S. Plot. The Onera elsA CFD software: input from research and feedback from industry. *Mechanics & Industry*, 14(3):159–174, 2013.
- [2] K. O. Dağ and J. N. Sørensen. A new tip correction for actuator line computations. *Wind Energy*, 23(2):148–160, 2020.
- [3] J. R. Forsythe, E. Lynch, S. Polsky, and P. Spalart. Coupled Flight Simulator and CFD Calculations of Ship Airwake using Kestrel. In *53rd AIAA Aerospace Sciences Meeting*, AIAA SciTech Forum. American Institute of Aeronautics and Astronautics, Jan. 2015.
- [4] H. Glauert. Airplane Propellers. In W. F. Durand, editor, *Aerodynamic Theory*, volume IV, pages 169–360. Springer, Berlin, Heidelberg, 1935.
- [5] S. S. A. Ivanell. Numerical Computations of Wind Turbine Wakes. Technical report, Jan. 2009.
- [6] A. Jameson, W. Schmidt, and E. Turkel. Numerical Solution of the Euler Equations by Finite Volume Methods Using Runge-Kutta Time Stepping Schemes. *AIAA Paper*, July 1981.
- [7] P. K. Jha, M. J. Churchfield, P. J. Moriarty, and S. Schmitz. Guidelines for Volume Force Distributions Within Actuator Line Modeling of Wind Turbines on Large-Eddy Simulation-Type Grids. *Journal of Solar Energy Engineering*, 136(3), Jan. 2014.
- [8] P. K. Jha and S. Schmitz. Actuator curve embedding an advanced actuator line model. *Journal of Fluid Mechanics*, 834:R2, Jan. 2018. Publisher: Cambridge University Press.
- [9] T. Kiffer, G. Dufour, R. Gojon, W. Thollet, and L. López de Vega. Extension and validation of the Body Force Method to a propeller blade. In *AIAA AVIATION 2023 Forum*, AIAA AVIATION Forum. American Institute of Aeronautics and Astronautics, June 2023.
- [10] J. C. Kok. Resolving the Dependence on Freestream Values for the k- Turbulence Model. *AIAA Journal*, 38(7):1292–1295, July 2000.
- [11] L. Martinelli and A. Jameson. Validation of a multigrid method for the Reynolds averaged equations. In *26th Aerospace Sciences Meeting*. American Institute of Aeronautics and Astronautics, 1988.
- [12] L. Martinez, S. Leonardi, M. Churchfield, and P. Moriarty. A Comparison of Actuator Disk and Actuator Line Wind Turbine Models and Best Practices for Their Use. In 50th AIAA Aerospace Sciences Meeting including the New Horizons Forum and Aerospace Exposition. American Institute of Aeronautics and Astronautics, 2012.
- [13] F. R. Menter. Two-equation eddy-viscosity turbulence models for engineering applications. *AIAA Journal*, 32(8):1598–1605, 1994.
- [14] R. Merabet and E. Laurendeau. Hovering Helicopter Rotors Modeling Using the Actuator Line Method. *Journal of Aircraft*, 59(3):774–787, May 2022.
- [15] B. Ortun. A coupled RANS/lifting-line analysis for modelling the aerodynamics of distributed propulsion. San Francisco, CA, 2018. AHS Technical Conference on Aeromechanics Design for Transformative Vertical Flight.
- [16] H. Pantel, F. Falissard, and G. Dufour. Assessment of Reynolds-Averaged Navier–Stokes/Blade Element Theory Body Force Method for Propeller Modeling. *AIAA Journal*, 62(2):758–775, 2024.
- [17] S. Péron and C. Benoit. Automatic off-body overset adaptive Cartesian mesh method based on an octree approach. *Journal of Computational Physics*, 232(1):153–173, Jan. 2013.
- [18] G. Reboul, D. Lewis, M. Balmaseda, J. Bailly, F. Falissard, F. Guntzer, and C. Lienard. Multi-fidelity Aeroacoustic Prediction of an eVTOL Rotor. In *Vertical Flight Society's 79th Annual Forum and Technology Display*, West Palm Beach, FL, May 2023.
- [19] W. Z. Shen, J. N. Sørensen, and R. Mikkelsen. Tip Loss Correction for Actuator/Navier–Stokes Computations. *Journal of Solar Energy Engineering*, 127(2):209–213, Apr. 2005.
- [20] M. Shives and C. Crawford. Mesh and load distribution requirements for actuator line CFD simulations. *Wind Energy*, 16(8):1183–1196, 2013.
- [21] T. C. A. Stokkermans, N. van Arnhem, T. Sinnige, and L. L. M. Veldhuis. Validation and Comparison of RANS Propeller Modeling Methods for Tip-Mounted Applications. *AIAA Journal*, 57(2):566–580, 2019.
- [22] J. Sørensen and W. Z. Shen. Numerical Modeling of Wind Turbine Wakes. *Journal of Fluids Engineering*, 124(2):393–399, May 2002.
- [23] W. Thollet, G. Dufour, X. Carbonneau, and F. Blanc. Body-force modeling for aerodynamic analysis of air intake fan interactions. *International Journal of Numerical Methods for Heat & Fluid Flow*, 26(7):2048–2065, 2016.
- [24] R. Wickersheim, M. Keßler, and E. Krämer. Noise Prediction of a Distributed Propulsion System Using the Actuator Line Method. *AIAA Journal*, 62(3):1123–1135, Mar. 2024.